JTTEE5 10:337-350

Erosion Resistance of Arc-Sprayed Coatings to Iron Ore at 25 and 315 °C

S. Dallaire, H. Levert, and J.-G. Legoux

(Submitted 14 February 2000; in revised form 10 June 2000)

Iron ore pellets are sintered and reduced in large continuous industrial oil-fired furnaces. From the furnace, powerful fans extract large volumes of hot gas. Being exposed to gas-borne iron ore particles and temperatures ranging between 125 and 328 °C, fan components are rapidly eroded. Extensive part repair or replacement is required for maintaining a profitable operation. The arc spraying technique has been suggested for repair provided it could produce erosion-resistant coatings. Conventional and cored wires (1.6 mm diameter) were arc sprayed using various spray parameters to produce 250 to 300 μm thick coatings. Arc-sprayed coatings and reference specimens were erosion tested at 25 and 315 °C and impact angles of 25 and 90° in a laboratory gas-blast erosion rig. This device was designed to impact materials with coarse (32 to 300 μm) iron ore particles at a speed of 100 m/s. The coating volume loss due to erosion was measured with a laser profilometer built by National Research Council Canada several years ago.

Few arc-sprayed coatings exhibited erosion resistance comparable with structural steel at low impact angles. Erosion of arc-sprayed coatings and reference specimens dramatically increases at 315 °C for both 25° and 90° impact angles. Erosion-enhanced oxidation was found to be responsible for the increase in volume loss above room temperature. Though arc spraying can be appropriate for on-site repair, the development of more erosion-resistant coatings is required for intermediate temperatures.

Keywords arc spray process, ASTM test method, cored wires, erosion resistance, microstructure

1. Introduction

Erosion is the main cause of failure of fans that evacuate or circulate hot gas from the oil-fired furnaces used to sinter and reduce iron ore pellets. Furnace gases reaching 1300 °C in the central part of the furnace easily raise the temperature of these fans up to 328 °C (Fig. 1). Gas-borne iron ore particles and pellet fragments, mainly composed of hematite (Fe_2O_3), are aspirated by these powerful fans and impact components at various impingement angles. Damage results from particle impact at nearly normal angles with some entrance components and at low angles with 900 rpm rotating blades. As the gas velocity can reach 100 m/s, solid particles are centrifuged against steel components, resulting in pronounced tip blade damage (Fig. 2). Erosion damage considerably shortens the lifetime of fans that are designed to last 10 years. Extensive and expensive repair is required and complete cooldown and startup line cycles cause important production loss.

To reduce maintenance time and improve repair efficiency, arc spraying has been proposed instead of tedious weld repair. Over other thermal spraying techniques, it offers higher deposition rate of materials, simplicity of operation, and lower toxic gas emission, making it suitable for on-site operation, particularly in a confined environment. This study was aimed at evalu-

S. Dallaire, H. Levert, and **J.-G. Legoux,** Industrial Materials Institute, National Research Council, Boucherville, PQ, Canada J4B 6Y4. Contact e-mail: serge.dallaire@nrc.ca.

Table 1 Commercial wires used for producing arc-sprayed coatings

Code	Coating type	Composition(a)	Supplier
W1	Austenitic stainless steel	0.1C, 18–20Cr, 8–12Ni, 2.0Mn, 0.7–1.0Si, Fe bal	Praxair Inc., Appleton, WI
W2	Martensitic stainless steel	16–18Cr, 0.95–1.2C, 1.0 Mn, 1.0Si, 0.75Mo, Fe bal	Aerospace Alloy, New York, NY
W3	Steel containing oxides	94.5Fe, 1.9Mn, 1.1 O_2, 2.5 other (not specified)	Praxair Inc., Appleton, WI
CW1	Chromium-rich steel	…	Praxair Inc., Concord, NH
CW2	Nickel-based alloy containing fine boride and carbide particles	0.8C, 15Cr, 3B, 4Si, 3.5Fe, 17.3W, Ni bal	Wall Colmonoy, Madison Heights, MI
CW3	Ferritic steel containing amorphous phases	1.7Si, 28.0Cr, 2.0Mn, 3.7B, Fe bal	Amorphous Technologies International, Laguna Niguel, CA
CW4	Duplex steel containing amorphous phases	8.4Cu/Ni, 1.8Si, 21.0Cr, 6.5Ni, 1.0Mn, 2.5B, 0.2C, Fe bal.	Amorphous Technologies International
CW5	Ferritic stainless steel containing titanium and tungsten carbide particles	1.2Si, 14.0Cr, 4.5Ni, 0.6Mn, 1.9B, 26.0WC, 6.0TiC, Fe bal.	Amorphous Technologies International
CW6	WC-Co particles embedded in a hardened steel	…	Metallisation Limited Dudley, England

(a) Composition given by the supplier

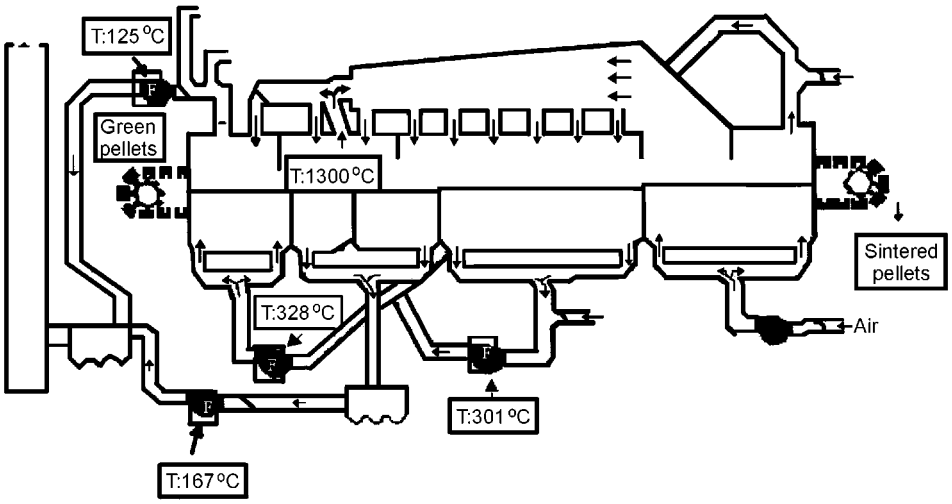

Fig. 1 Schematic of the furnace used to sinter iron ore pellets

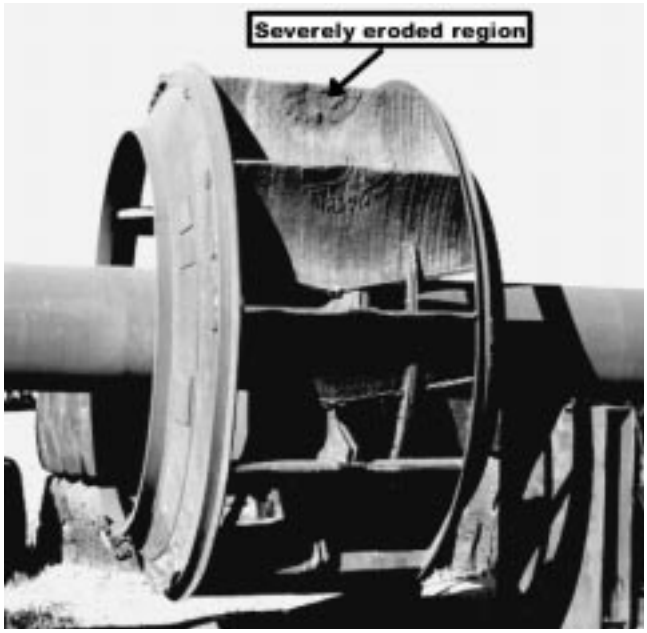

Fig. 2 Photograph of a worn fan rotor showing damaged blades

ating selected arc-sprayed coatings for protecting fan components in a laboratory-scale gas-blast erosion rig, simulating conditions in fans, and at determining the level of improvement they offer over conventional construction steel.

2. Experimental Procedure

2.1 Arc-Sprayed Coatings and Materials

Four conventional and five cored wires (1.6 mm diameter) were arc sprayed. The chemical composition and the suppliers

Table 2 Arc spraying parameters

Wire identification	Spraying condition	Arc voltage (V)	Arc amperage (A)	Spray distance (mm)	Traverse speed (mm/s)	Spray rate (kg/s × 10^{-2})
W1	1	27	200	100	305	7.65
W1	2	27	200	200	610	7.65
W1	3	29	200	100	610	8.12
W1	4	29	200	200	305	8.12
W2	1	30	200	100	305	6.32
W2	2	30	200	200	610	6.32
W2	3	32	200	100	610	6.77
W2	4	32	200	200	305	6.77
W3	1	30	200	100	305	5.53
W3	2	30	200	200	610	5.53
W3	3	32	200	100	610	5.30
W3	4	32	200	200	305	5.30
CW1	1	31	150	100	305	4.73
CW1	2	31	150	200	610	4.73
CW1	3	33	150	100	610	4.62
CW1	4	33	150	200	305	4.62
CW2	1	29	150	100	305	5.73
CW2	2	29	150	200	610	5.73
CW2	3	31	150	100	610	5.18
CW2	4	31	150	200	305	5.18
CW3	1	34	175	100	305	6.20
CW3	2	34	175	200	610	6.20
CW3	3	36	175	100	610	5.68
CW3	4	36	175	200	305	5.68
CW4	1	30	150	100	305	4.63
CW4	2	30	150	200	610	4.63
CW4	3	32	150	100	610	4.43
CW4	4	32	150	200	305	4.43
CW5	1	30	150	100	305	4.93
CW5	2	30	150	200	610	4.93
CW5	3	32	150	100	610	4.45
CW5	4	32	150	200	305	4.45
CW6	1	30	150	100	305	3.83
CW6	2	30	150	200	610	3.83
CW6	3	32	150	100	610	3.78
CW6	4	32	150	200	305	3.78

Air pressure fixed at 550 kPa
Distance between successive passes maintained at 10 mm

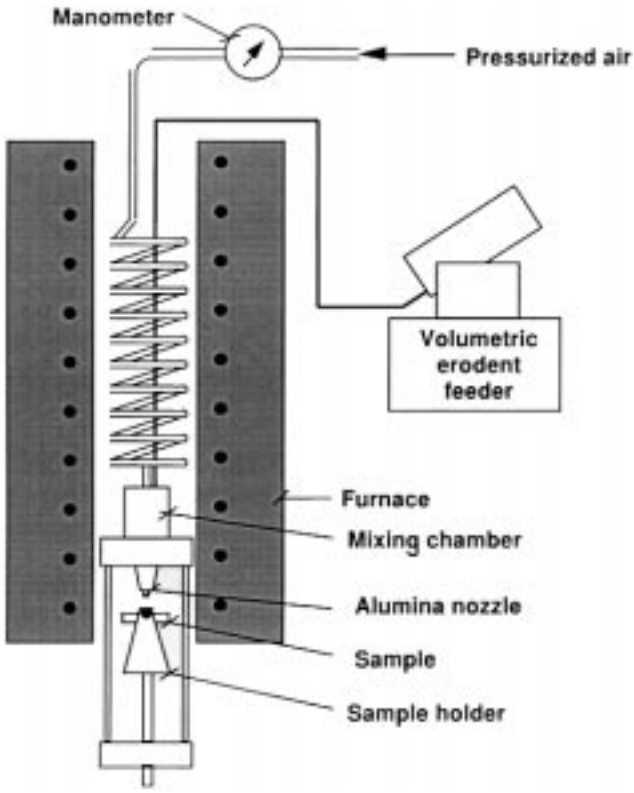

Fig. 3 Schematic of the gas blast erosion device

Table 3 Gas-blast erosion parameters

Erodent particles	Iron ore (32 to 300 μm)
Particle flow rate	4.4×10^{-5} ($\pm$5%) kg s^{-1}
Mean velocity of particles	97 ($\pm$5%) m s^{-1}
Erosion test duration	300 s
Test temperatures	25 ($\pm$5) and 315 ($\pm$15) °C

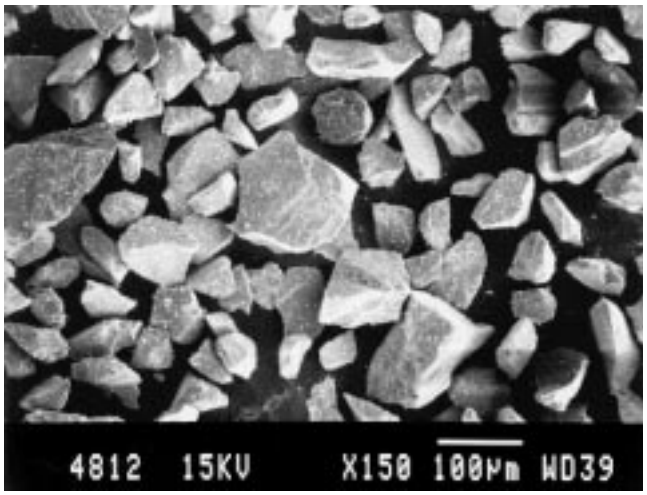

Fig. 4 Scanning electron micrograph of iron ore particles

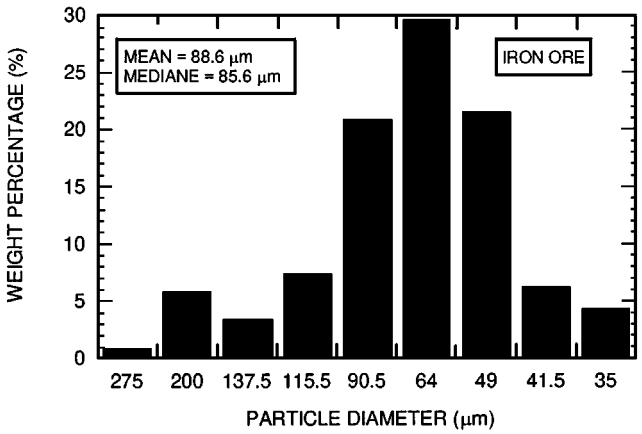

Fig. 5 Size distribution of iron ore particles used in the erosion tests

of these wires are listed in Table 1. Arc spraying of these wires would produce coatings based on the following:

- steel (W3) and chromium-rich steel (CW1),
- carbon-rich steel with tungsten carbide particles (CW6),
- austenitic (W1) and martensitic (W2) stainless steel,
- ferritic (CW3 and CW5) and pseudoduplex (CW4) stainless steels containing hard phases, and
- nickel-based alloy containing fine boride and carbide particles (CW2).

All wires were arc sprayed using a Miller BP 400 arc spray system (Appleton, WI) with 550 kPa air pressure. Spraying parameters were selected anticipating on-site deposition with a hand-operated spray torch. The arc voltage, spray distance, and transverse spray speed were considered. Two levels of variation for parameters were selected, and deposition experiments were carried out to fit a L4 (2^n) Taguchi matrix. All of the spraying parameters are summarized in Table 2. The effect of spray parameters was analyzed using standard procedures for a Taguchi-type matrix: effects of parameter X = (sum of the response for parameter X at level 1–sum of the response for parameter X at level 2)/2.

The spray rate was determined by weighing portions of wire fed to the torch over a fixed period of time with potentiometer settings corresponding to the arc currents shown in Table 2. Coatings with a thickness of 300 μm were deposited on 100 $\times$ 100 $\times$ 3 mm grit-blasted (alumina, 24 grit, and 275 kPa air pressure) mild steel pieces. Cooling was not provided on the back face of steel substrates nor was any gas used to cool coatings or sweep away oversprayed particles to simulate on-site spraying. For comparison purposes, AISI 1045 normalized steel, 316 stainless steel, and electrolytic tough pitch (ETP) copper specimens were also erosion tested. Arc-sprayed coatings and reference specimens were diamond ground to obtain flat surfaces and uniform roughness ($R_a \cong 2$ μm) prior to erosion testing.

2.2 Erosion Testing

Arc-sprayed coatings and reference specimens were erosion tested at impact angles of 25 and 90° and temperatures of 25 and

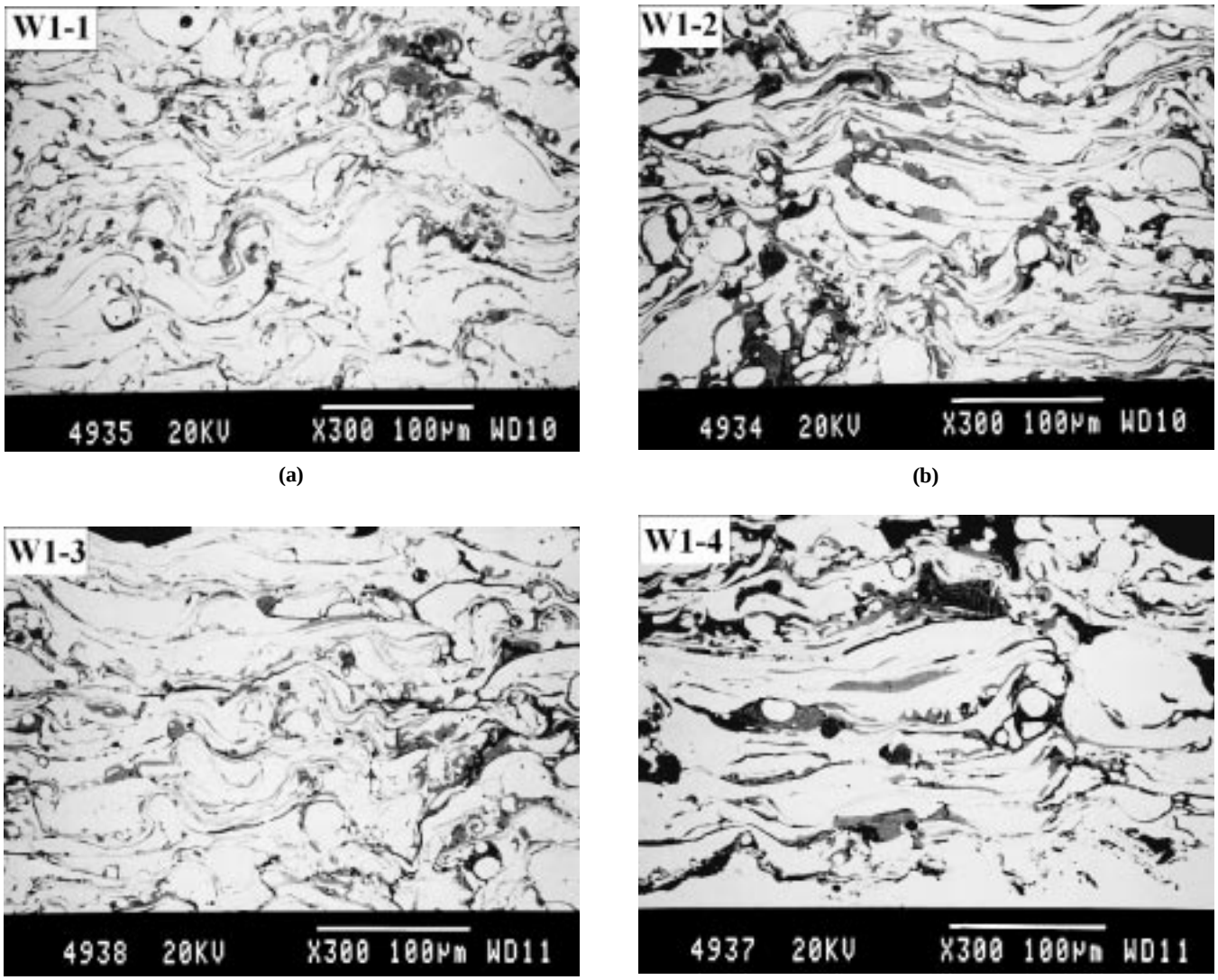

Fig. 6 W1 coating microstructure, SEM backscatered electron image

315 °C using a laboratory gas-blast erosion device (Fig. 3). In this method, particles were accelerated in a gas stream along a nozzle before impacting the tested specimen. The design of this laboratory erosion device[1] was based on materials contained in Ref 2 to 4.

From the mixing chamber, the particle stream was accelerated and focused on the target located at 10 mm from the end of the alumina nozzle. An impact area of 7 mm^2 at an impingement angle of 90° was obtained with an alumina nozzle with an internal diameter of 1.6 mm. A constant particle flow rate to the mixing chamber was ensured by a volumetric powder feeder. The particle flow rate was fixed at 4.4×10^{-5} kg s^{-1}, giving a particle flux of 6.22 kg m^{-2} s^{-1}, a value below the flux required to avoid interparticle interaction.[5] Three hundred second test durations with this particle flux were adequate to obtain steady-state erosion rates and to avoid eroding through the coating thickness.

Iron ore collected from the dust collectors was used as an erodent. Prior to testing, the iron ore was oven dried and sieved. The -32 μm fraction was removed, fines being very difficult to convey in the erosion testing device and being considered less damaging in erosion.[6] Figure 4 shows the angular morphology of the iron ore particles used in erosion tests, and Fig. 5 shows the particle size distribution, which ranges between 32 and 300 μm, with a mean particle size of 89 μm. Due to their parallelepiped shape (Fig. 4), the iron ore particles could go through a particular sieve for a small variation in minor axis size. This explains the apparent bimodal particle size distribution observed in Fig. 5.

The air driving pressure required to obtain a mean particle velocity of the order of 100 m s^{-1} was determined by measuring particle velocities 10 mm from the end of the alumina nozzle, where the target would be located. Particle velocities were measured with the DPV-2000 apparatus (Tecnar, Boucherville, Canada). This optical sensing device was previously designed to measure the speed of particles during spraying[7] and was modified to measure large non-light-emitting particles in this case. An air pressure of 414 kPa was required to ensure a mean particle velocity of 103.3 m s^{-1} based on particle velocity counts. The true particle stream mean velocity defined by

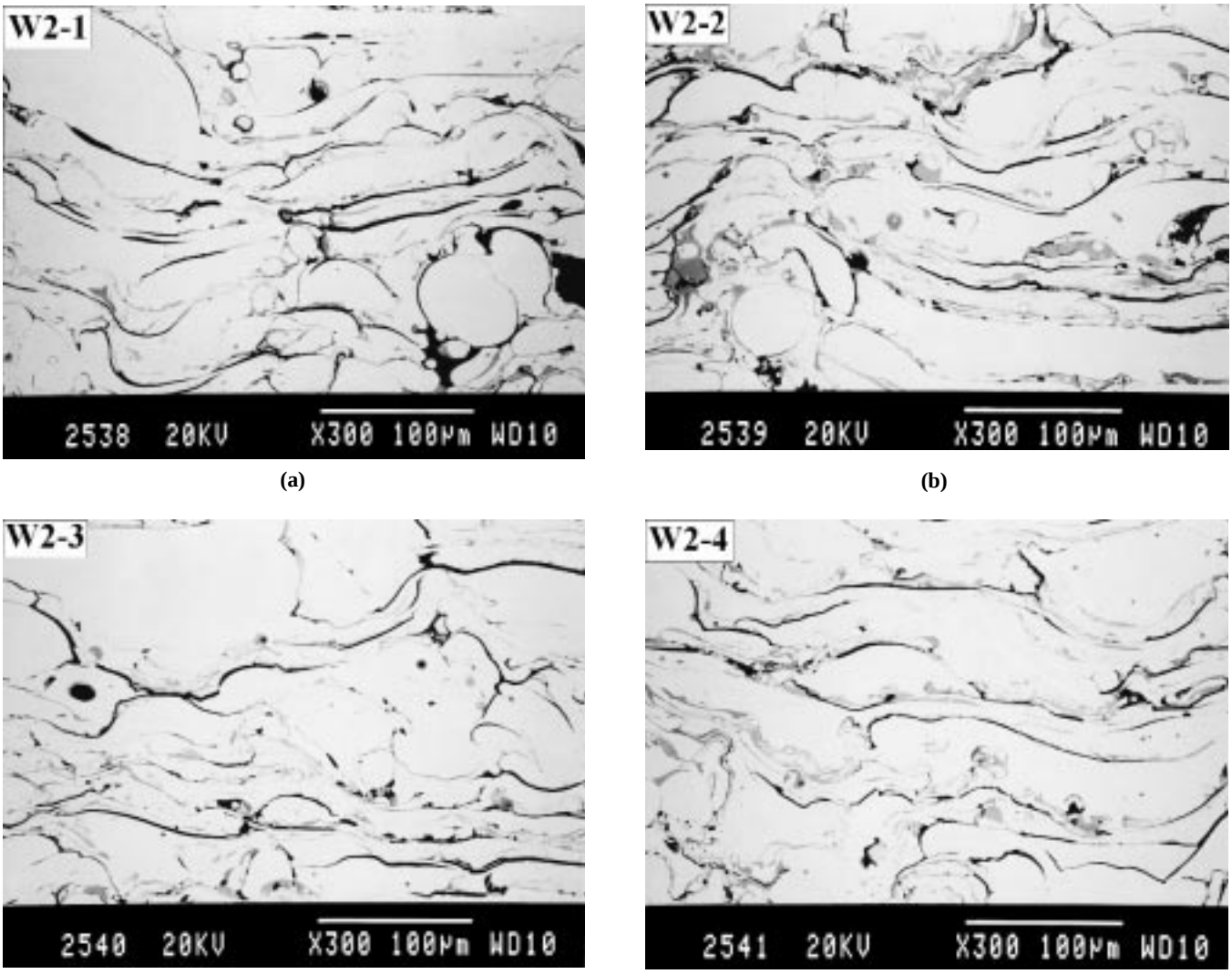

Fig. 7 W2 coating microstructure, SEM backscatered electron image

fluid flow equations[8] was 97 m s^{-1}, the highest velocity being 115 m s^{-1} in the middle of the stream and 79 m s^{-1} on the edge.

Before tests were carried out at a given temperature, the furnace was previously heated to a determined temperature higher than the test temperature. The sample holder was then introduced at the bottom of the furnace, compressed air heated within the coil ensuring that the target reached the required temperature before introducing particles. The target temperature was recorded during tests with a 0.5 mm diameter subminiature thermocouple probe (Omega Engineering Inc., Stanford, CT) fixed at the back face of the sample. Table 3 summarizes the test parameters used in the erosion tests.

To ensure test reproducibility, measurements of particle flow rate and nozzle diameter were done when introducing a new lot of iron ore in the erosion device. Enlargement of the erosion crater diameter indicated deviations in erosion rate.[9] When noticeable differences were observed, the erosion device required a calibration. In all measurements, the mean particle flow rate was 4.4×10^{-5} kg/s with a standard deviation inferior to 5% for

Table 4 Effect of spray parameters on the erosion properties of coatings

		Effect		
Wire Identification	**Property**	**Arc voltage (low-high)/2**	**Spray distance (short-long)/2**	**Traverse speed (slow-fast)/2**
W1	Erosion 25°	−5.645	−7.305	0.265
(SS1 316)	Erosion 90°	3.37	−7.76	0.72
W2	Erosion 25°	5.49	2.23	−2.46
(440C)	Erosion 90°	8.325	−1.515	0.075
W3	Erosion 25°	2.465	−14.275	−1.405
(Tufton)	Erosion 90°	5.34	−20.19	−2.62
CW1	Erosion 25°	1.175	−0.565	0.795
(95 MXC)	Erosion 90°	4.805	9.055	3.065
CW2	Erosion 25°	1.97	−2.12	2.96
(Colmonoy 88)	Erosion 90°	5.49	−1.4	4.43
CW3	Erosion 25°	9.7	4.77	3.63
(Armacor M)	Erosion 90°	22.73	8.86	0.68
CW4	Erosion 25°	2.95	−2.12	3.18
(Armacor 16)	Erosion 90°	0.835	−1.975	2.275
CW5	Erosion 25°	−16.55	−32.84	−18.52
(Duocor)	Erosion 90°	−9.55	−28.71	−42.88
CW6	Erosion 25°	5.83	−4.62	−0.91
(97T)	Erosion 90°	−5.605	−10.905	2.275

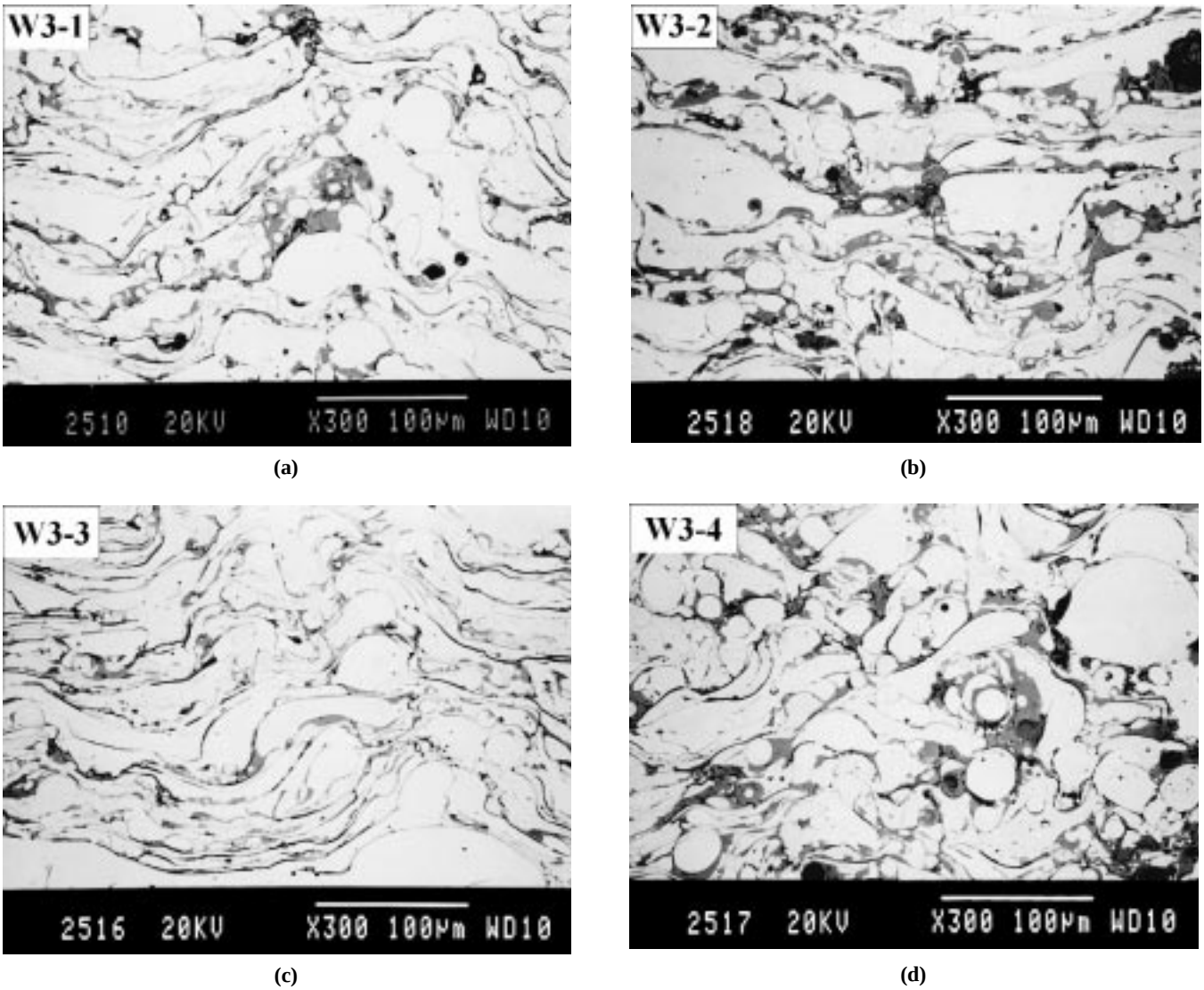

Fig. 8 W3 coating microstructure, SEM backscatered electron image

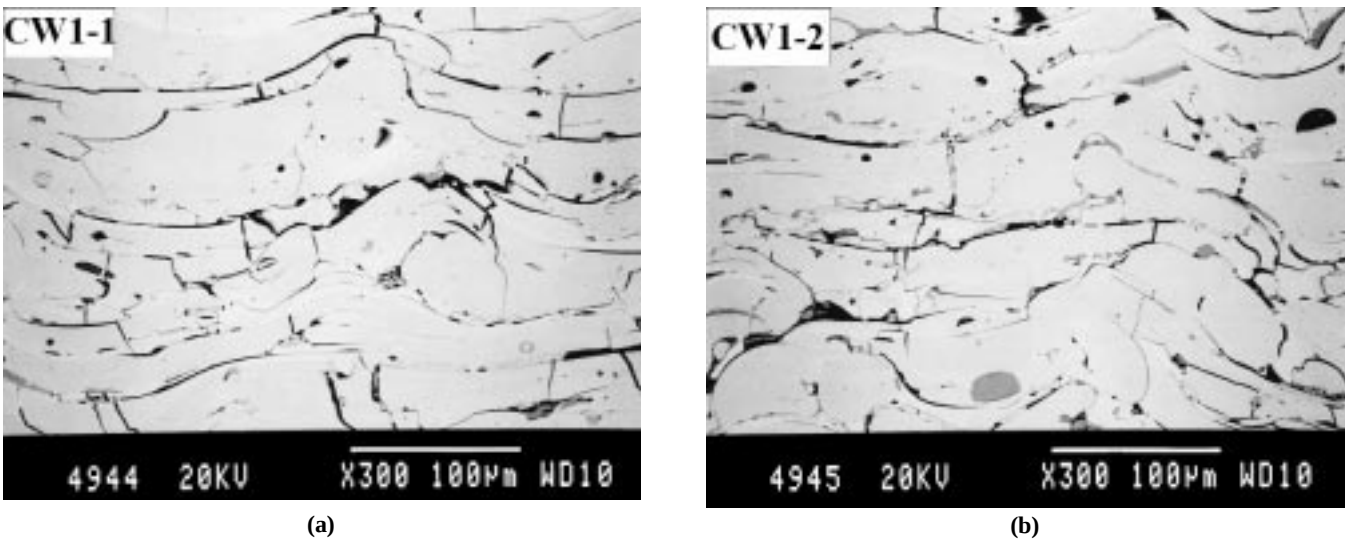

Fig. 9 CW1 coating microstructure, SEM backscatered electron image (continued on next page)

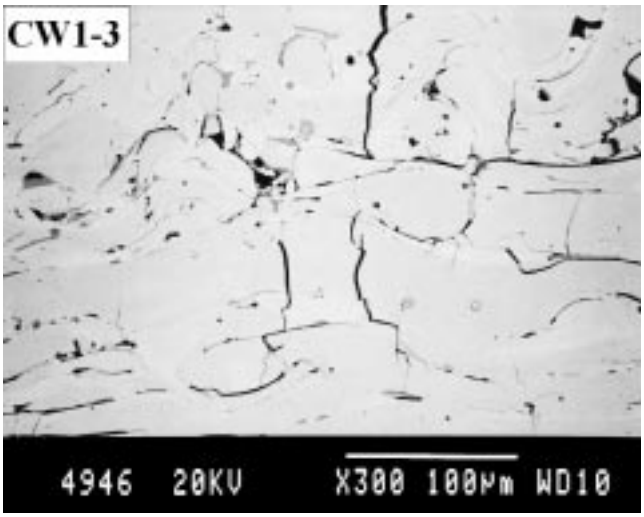

(c)

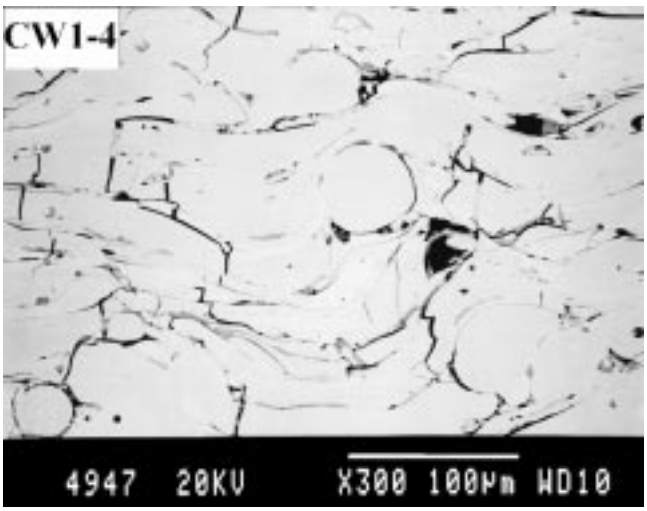

(d)

Fig. 9 (continued) CW1 coating microstructure, SEM backscatered electron image

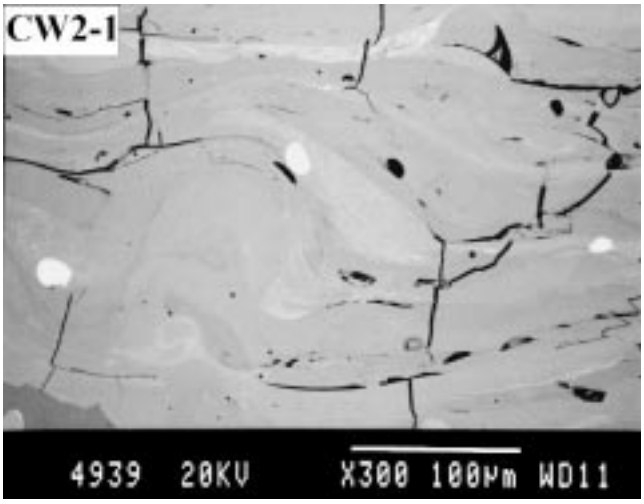

(a)

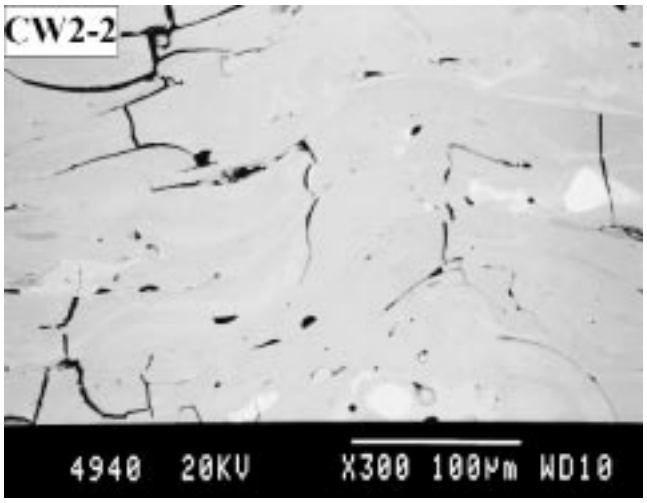

(b)

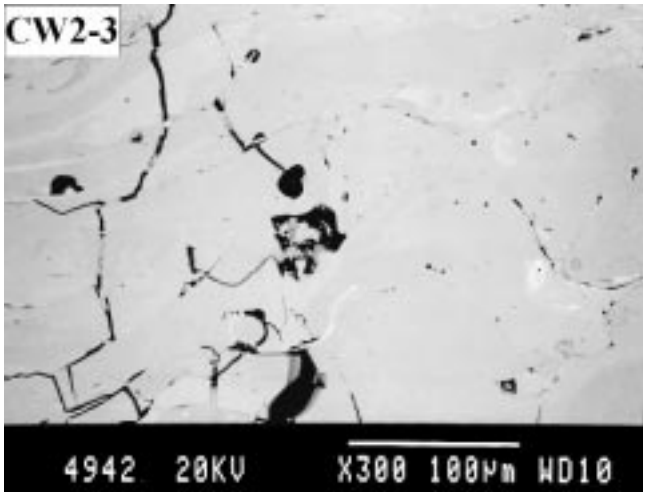

(c)

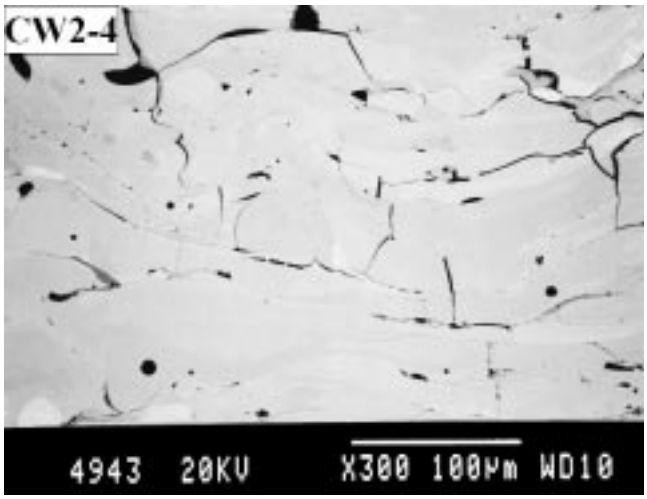

(d)

Fig. 10 CW2 coating microstructure, SEM backscattered electron image

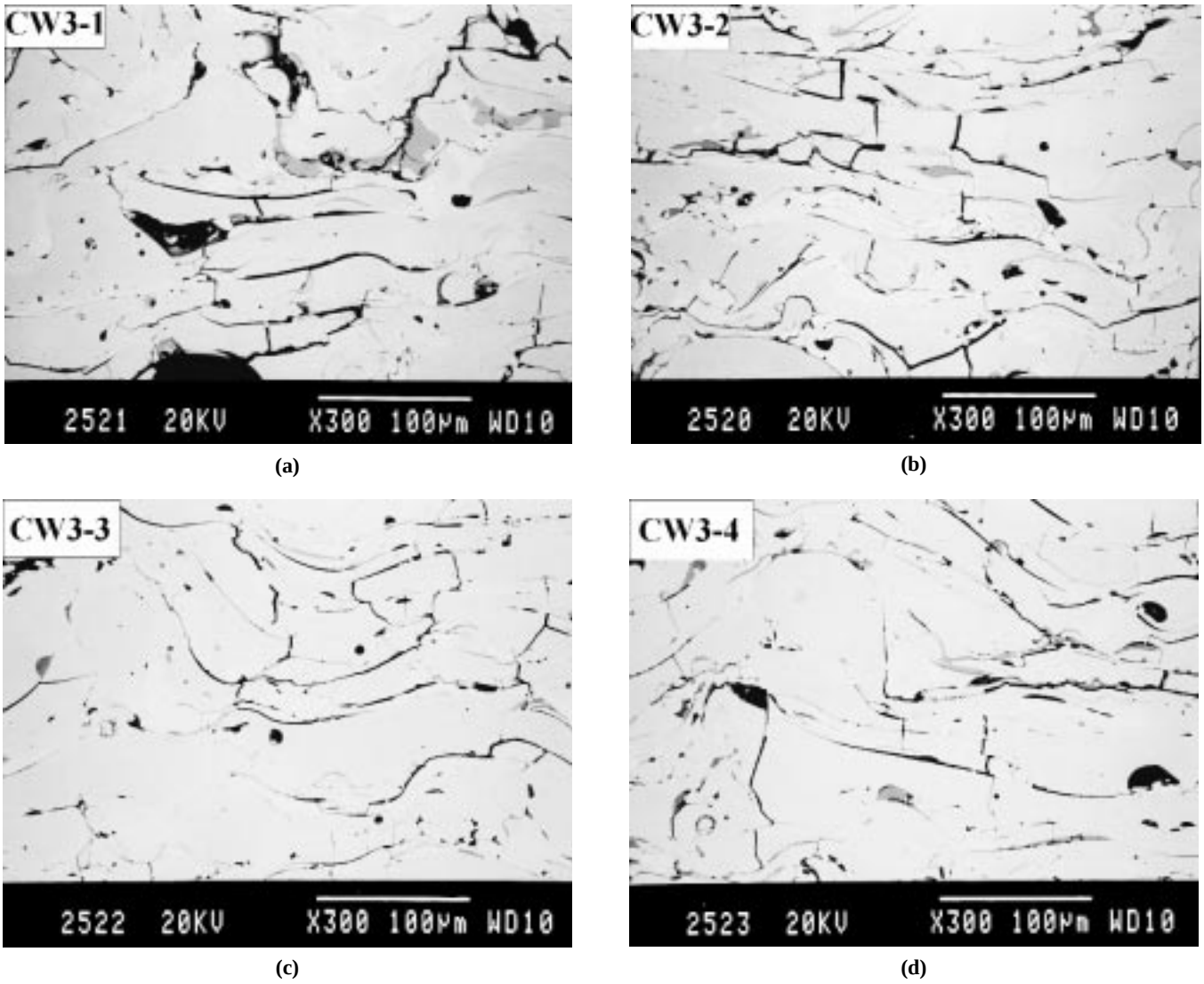

Fig. 11 CW3 coating microstructure, SEM backscattered electron image

75 flow rate measurements. Diameter enlargements of both the nozzle and impact area were not noticed after the complete evaluation of sprayed coatings.

2.3 Erosion Evaluation

Before volume loss measurements, samples were ultrasonically cleaned in propanol and oven dried at 100 °C. Erosion was reported as coating volume loss per kilogram of impacting erodent particles (mm^3/kg of iron ore). The volume loss took into account both coating density differences, erosion damage, and defects already present within coatings before erosion testing. The volume loss measurements and erosion damage evaluation were performed with a laboratory optical profilometer like the one described before.[10] This apparatus is mainly composed of (a) a laser diode source projecting visible light at one point of the surface along a direction perpendicular to the surface, (b) a charge-coupled device camera for collecting the light scattered by the surface 45° away from the lighting source, and (c) an *X-Y* displacement system composed of two motor-driven linear slides. For an irregularly worn surface, height resolution greater than 5 μm, within a 2 mm range, is achieved. The evaluation of the volume loss on worn materials could be done with an accuracy greater than 1%, the accuracy between the wear volume losses performed on different samples being better than 10%.

2.4 Microstructure Observation

Microstructure observations were done on the cross sections of coatings produced with various spray parameters. Observation was performed after diamond cutting, infiltration, and proper polishing, ensuring the preservation of the coating microstructure. Observations were done with scanning electron microscopy (SEM). A backscattered electron image was used to enhance the chemical contrast.

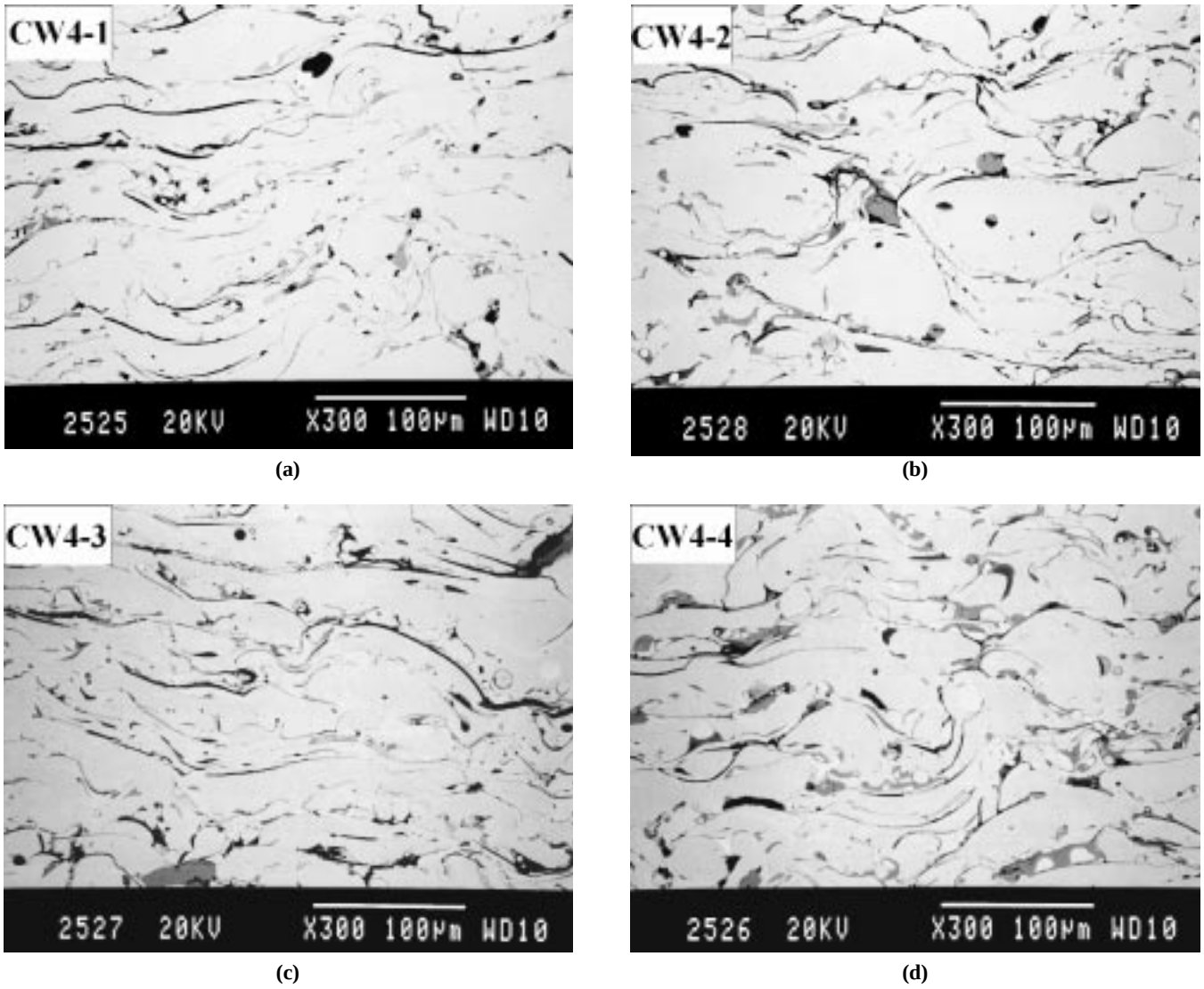

Fig. 12 CW4 coating microstructure, SEM backscattered electron image

2.5 Hardness Measurements

Diamond pyramid hardness measurements were performed with a Knoop indenter on diamond-polished cross sections of coatings and conventional materials using a small load of 25 g in order to match the indenter mark with the small microstructural features found in coatings. Results are reported as means of measurements taken at 50 μm intervals from the substrate. Depending on the coating thickness, more than seven measurements were done. Isolated hard phases (hardness$>$ 2000 kgf mm^{-2}) found in coatings were attributed to blasting or polishing particles and, therefore, were not considered in the reported values.

3. Results

3.1 Microstructure

The microstructure of coatings manufactured using the spray conditions described in Table 2 are presented in Fig. 6 to 14. Three different types of microstructures were identified. The first type, comprising the coatings W1 and W3, consists of metal-sprayed droplets surrounded by oxide stringers. The second group is also constituted of metal-sprayed droplets with very little or no oxide between splats. The absence of oxide stringers in these four coatings is most likely due to the presence of carbon or boron, which act as deoxidizers during spraying, preventing the formation of solid oxide around the flattening particles. In this group, coatings W2 and CW4 present some interlamellar cracks, although the coatings CW1 and CW3 present extensive vertical cracking. The third type of microstructure represented by CW5 and CW6 coatings consists of a multiphase matrix structure. The CW5 coating presents more interlamelar cracks than the CW6 coating. The coating CW2 can be considered as a combination of types 2 and 3. It contains second phases with a lesser volume fraction than type 2. The absence of oxide stringers as well as the extensive vertical cracking of type 2 coatings was observed.

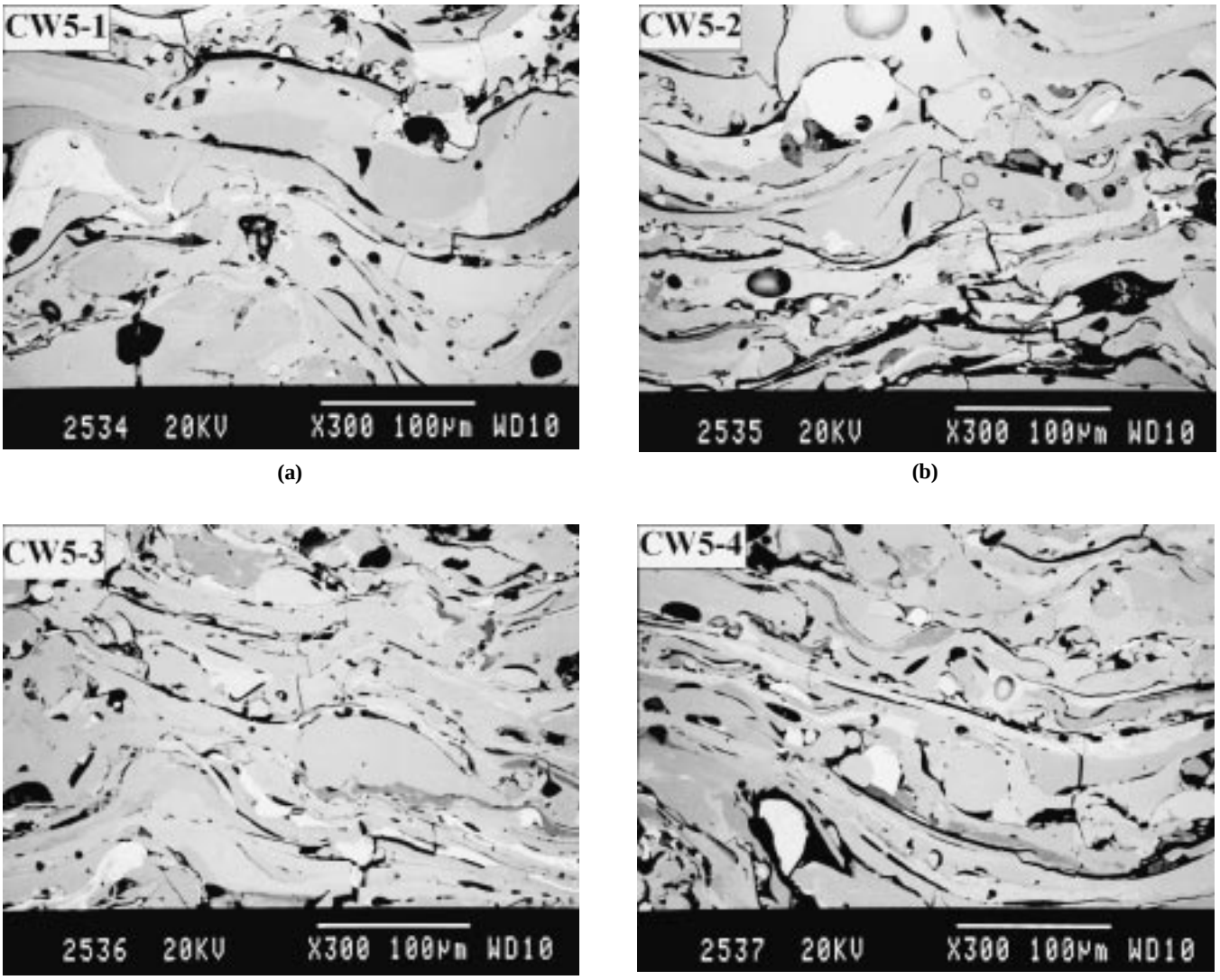

Fig. 13 CW5 coating microstructure, SEM backscattered electron image

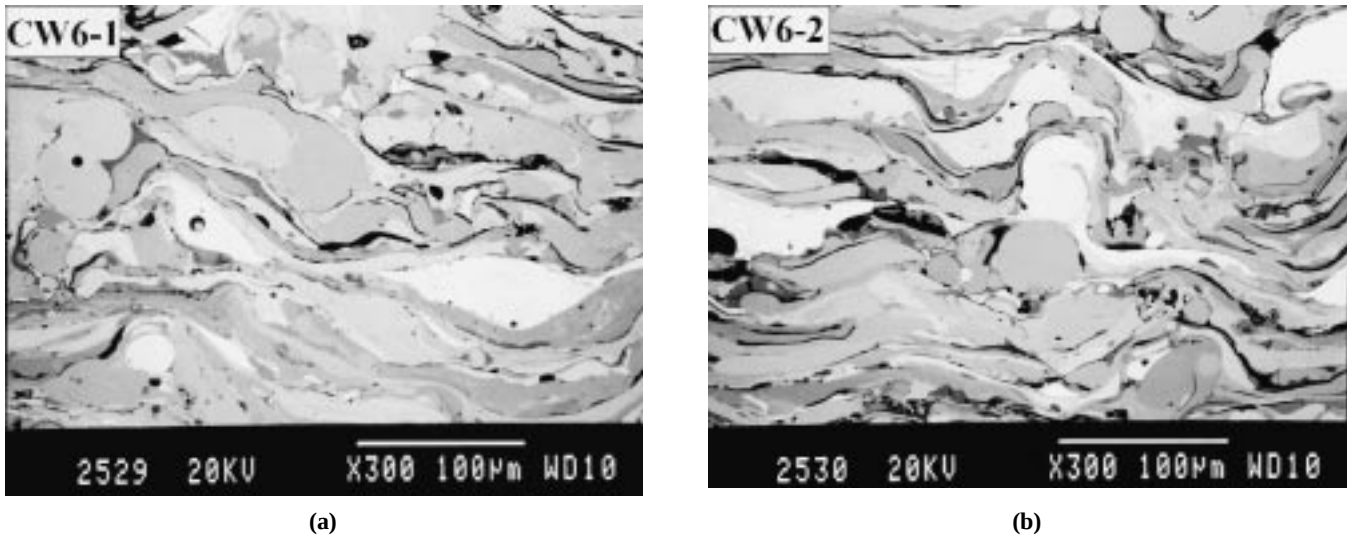

Fig. 14 CW6 coating microstructure, SEM backscattered electron image (continued on next page)

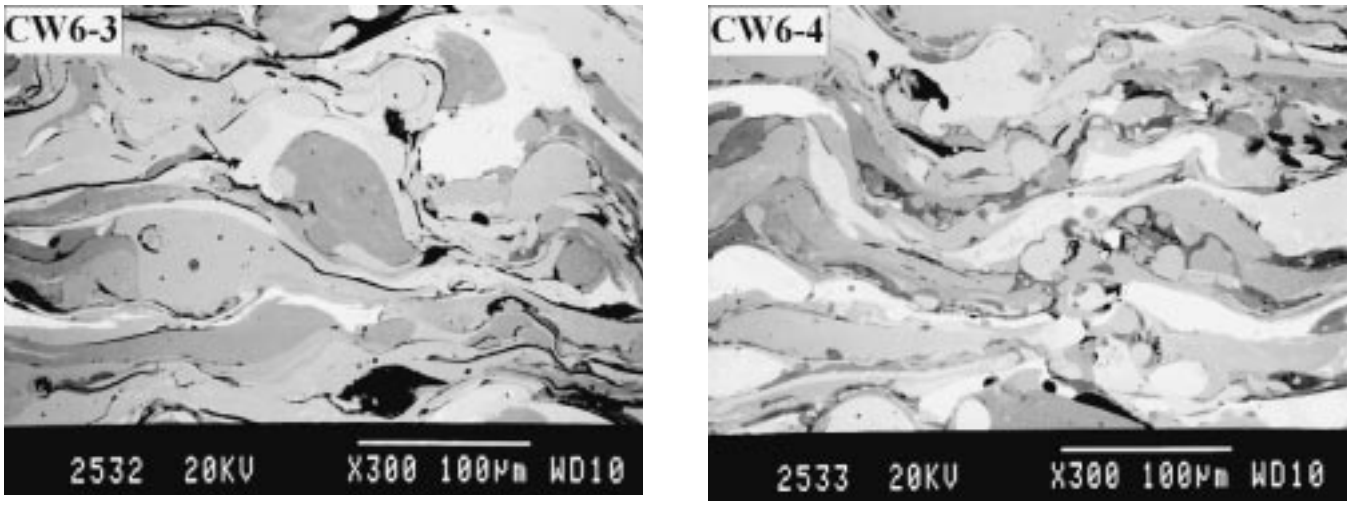

(c) (d)

Fig. 14 (continued) CW6 coating microstructure, SEM backscattered electron image

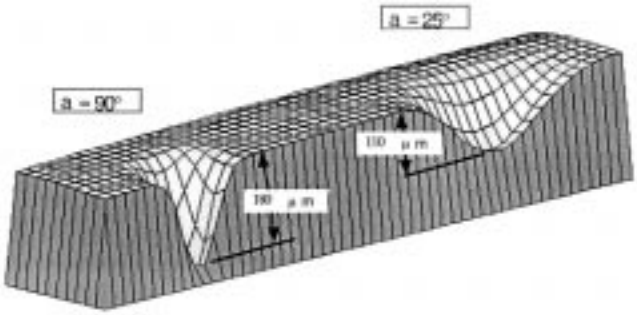

Fig. 15 Cross sections of erosion depth profiles in 316 stainless steel

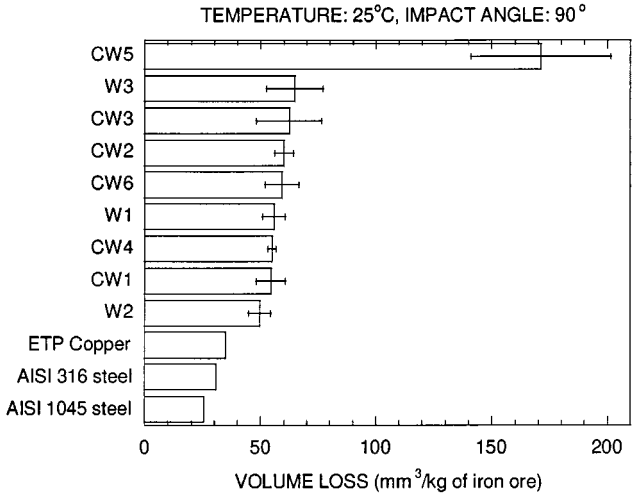

Fig. 16 Volume loss materials at an impact angle of 90° at 25 °C of arc-sprayed coatings and reference. Error bars correspond to the smallest and largest volume losses of coatings sprayed with parameters listed in Table 2

Quantifying the different microstructural feature is troublesome. In type I coatings, the oxide content can be related to the spray distance; the coatings obtained using spray conditions 2 and 4 for both W1 and W3 coatings contain a lot more oxides than those produced using conditions 1 and 3. For the two other types, it is not possible to quantify the effect of spray parameters.

3.2 Forms of Erosion Craters

The impacting iron ore particles dug craters with different shapes and depths depending on impact angles. The impact areas were as follows: at the impact angle of 90°, a circle having a 3 mm diameter; and, at the impact angle of 25°, an ellipse having a minor axis of 4 mm and a major axis of 8 mm (Fig. 15).

3.3 Erosion at Room Temperature

At room temperature, the erosion volume loss of arc-sprayed coatings depended strongly on the impact angle, as shown in Fig. 16 and 17. At an impact angle of 90°, all of the coatings exhibited volume losses of about 55 mm^3/kg of iron ore, except the CW5 coating, which exhibited a volume loss of 170 mm^3/kg of iron ore (Fig. 16). At an impact angle of 25°, arc-sprayed coatings exhibited volume losses ranging between 40 and 70 mm^3/kg, and CW1 and CW3 coatings exhibited the lowest volume losses of 40 to 50 mm^3/kg (Fig. 8). Figure 16 and 17 also indicate which variation in volume loss results while spraying wires using the Taguchi experimental design with the parameters listed in Table 2. Deviations were different at impact angles of 25 and 90° and showed how spraying parameters could influence the erosion resistance.

The effects of spray parameters are described in Table 4. We can see that group 1 and 3 coatings are sensitive to the spray distance, the coating made using a shorter distance performing better than the coating obtained using a longer spray distance. For group 1 coating, this can be explained by the lower oxide content

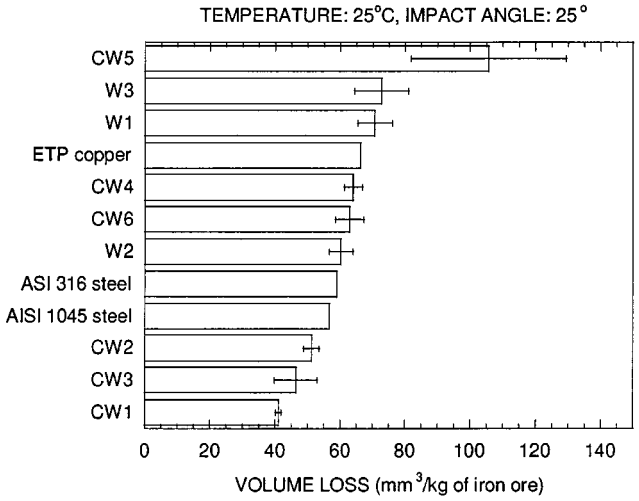

Fig. 17 Volume loss at an impact angle of 25° at 25 °C of arc-sprayed coatings and reference materials. Error bars correspond to the smallest and largest volume losses of coatings sprayed with parameters listed in Table 2

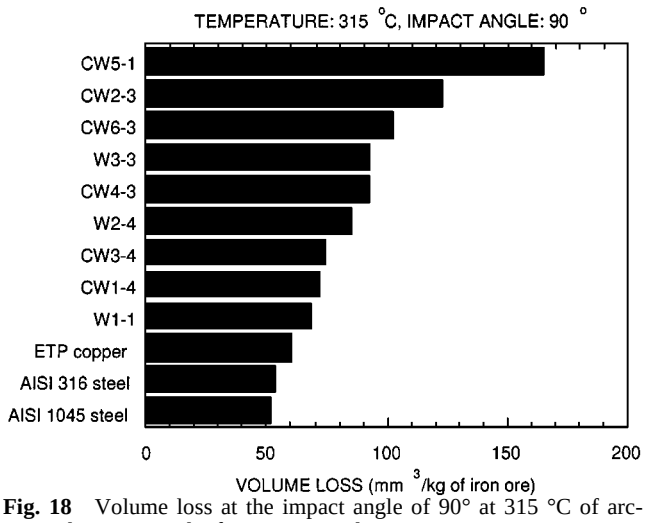

Fig. 18 Volume loss at the impact angle of 90° at 315 °C of arc-sprayed coatings and reference materials

of the coating made at lower spray distance. The lower interlamellar oxide reduces the brittleness of the interlamellar region and, thus, increases the erosion wear resistance of the coatings. The reason for the better performance in coatings CW5 and CW6 when produced using a shorter spray distance is less clear. For the coating of group 2, the influence of spray parameters on the properties is less clear. Coating W2 is more sensitive to arc voltage. Coatings CW1 and CW3 have similar behaviors and seem to be more affected by the erosion angle than by the spray parameters. This may be related to their crack patterns, which may be more solicited with a 90° erosion than with one at 25°.

For the spraying parameters listed in Table 2, the CW5 coatings exhibited the largest variations in erosion volume loss due to changes in spraying conditions. This can be related to the presence of more extensive interlamellar cracking present in these coatings (Fig. 13). However, it was not possible to relate the extent of the cracking to the variation of spray parameters.

3.4 Erosion at 315 °C

Coatings sprayed with parameters producing the best average erosion resistance at 25 °C were also tested at 315 °C. At this temperature, the volume loss markedly increased at both impact angles. Figure 18 shows that coatings exhibited volume losses ranging from 70 to 120 mm^3/kg of iron ore at an impact angle of 90°. Contrary to the tests carried out at room temperature, the difference in volume loss for the different coatings was more pronounced. At an impact angle of 25°, all the coatings exhibited twice the volume loss at 315 °C than at room temperature (Figures 17 and 19).

When compared with 1045 and 316 stainless steel and copper, coatings tested at 90° impact angle exhibited higher volume losses at 25 and 315 °C, although their rank was modified. For an impact angle of 25°, some arc-sprayed coatings exhibited lower volume losses than 1045 and 316 steels: CW1 and CW3 at 25 and 315 °C; and CW2 at 25 °C.

4. Discussion

4.1 The Role of Hardness and Strength in Erosion Protection at Low and High Particle Impact Angles

The capacity of materials to resist erosion depends upon the angle at which particles strike the surface. As schematically represented in Fig. 20,[11] to resist high speed particles impacting at high angles, materials must possess strength and also ductility to permit repeated deformation without loss of material. None of the coatings considered in this work resisted impacting particles at 90° better than 1045 steel, 316 stainless steel and ETP copper at 25 and 315 °C.

At low impact angles, there is a requirement for both hardness and toughness. Sprayed coatings produced from CW1, CW2, and CW3 wires exhibited slightly lower volume losses than 1045 steel at room temperature. As indicated in Fig. 21, these coatings were among those possessing the highest hardness at 25 °C. At 315 °C, CW1 and CW3 coatings exhibited lower volume loss than AISI 1045 steel. Coatings sprayed with W2, CW2, and CW5 wires exhibited equivalent volume loss to 316 stainless steel. These coatings exhibited the highest hardness at 25 °C (Fig. 21). Iron ore with a hardness of 1420 kg mm^2 is one of the hardest minerals found in the mining industry. Its hardness is higher than hematite (Fe_2O_3) and magnetite (Fe_3O_4) and is comparable to that of silica.[12]

To combat erosion, materials must be hard enough to deflect impacting particles at low angles and soft enough to absorb the energy of particles impacting at high angles. The conflicting properties of hardness and ductility are not naturally met in conventional materials. Attempts to further optimize the spray deposition of wires did not result in a significant overall improvement of coating erosion resistance.

4.2 The Effect of Temperature on Particle Erosion

It was observed that a rise in temperature to 315 °C resulted in a dramatic increase in volume loss for both the sprayed coat-

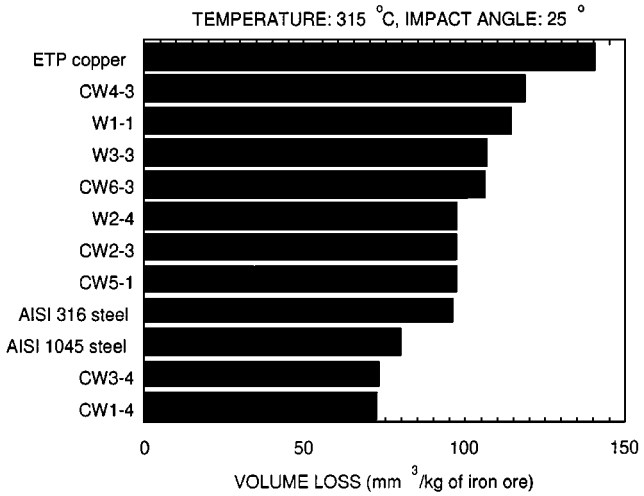

Fig. 19 Volume loss at the impact angle of 25° at 315 °C of arc-sprayed coatings and reference materials

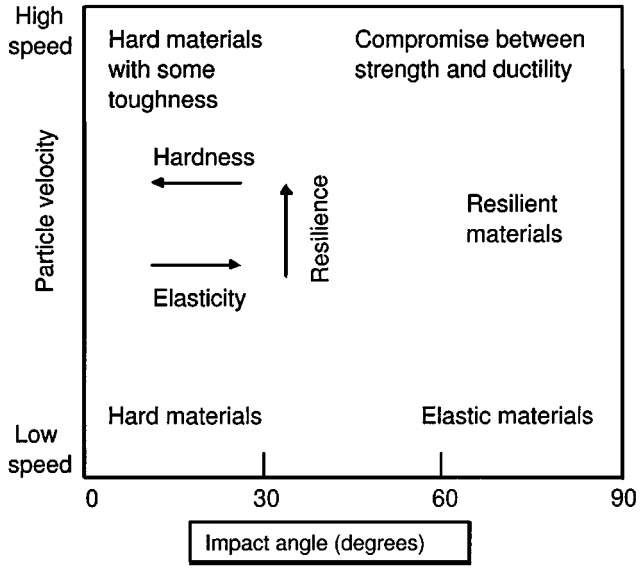

Fig. 20 Schematic guide for the selection of materials for resisting erosion according to particle speed and impact angle[11]

Table 5 Temperature for maximum erosion rate in commercial alloys[17–19](a)

Alloy	Temperature (°C)
Bright mild steel	300
3.3Cr-0.5Mo steel	400
1Cr-0.5Mo steel	400
Incoloy 800H	450
2.25Cr-1Mo steel	480
347 stainless steel	480

(a) Tests carried out in a fluidized bed with 240 μm alumina particles at a velocity of 2.5 m s^{-1}

ings and the reference materials. This increase in volume loss could not be attributed only to changes in mechanical properties with temperature. Indeed, the hardness of steel and stainless steel falls very slowly from room temperature to 315 °C.[13] The ETP copper loses a third of its hardness between 100 and 200 °C.[14] Erosion testing of 410 stainless steel in a gas blast rig using inert gas showed an erosion rate at 250 °C that was only 20% of its room-temperature value.[15] Sprayed coatings based on steel and stainless steel most likely increase their ductility as the temperature increases. However, this increase in ductility with temperature did not result in a lower volume loss at 315 °C for the 90° impact angle. Therefore, changes in mechanical properties with temperature cannot be completely responsible for the large volume losses observed at 315 °C, particularly at a 90° impact angle.

The large volume losses observed at 315 °C cannot be related to the so-called erosion-corrosion phenomenon observed at temperatures above 600 °C. For materials erosion tested at high temperatures, the oxide growth is usually slow and the oxide properties determine the erosion rate of materials. Protection against oxidation is afforded as long as the oxide is not removed by fracture at the scale-metal interface.

Under the conditions used in this work, oxidation was not severe enough to cause dramatic volume loss. For instance, under static oxidation conditions in air, the formation of a 2 μm thick oxide on 347 steel at 600 °C requires more than 3.6×10^5 s.[16] In fluidized bed combustors with particle velocity as low as 2.5 m s^{-1}, high levels of volume loss due to erosion for mild and low alloy steels were observed for temperatures comprised between 100 and 500 °C.[17–19] Large volume losses at 315 °C were, therefore, not only due to erosion but also largely to oxidation. At these intermediate temperatures, thin (a few tens of nanometers in thickness) oxide layers are formed at much greater rates than would be the case during static oxidation. Impacting particles repeatedly take off thin oxide layers, the exposed metallic surface being readily reoxidized. Therefore, above room temperature, erosion accelerates the oxidation of materials.

The erosion rate depends not only on the composition of targets but also on the velocity of the erodent. The temperature observed for the highest volume loss can be as low as 300 °C for mild steel and reaches 480 °C for 2.25Cr-1Mo, as shown in Table 5. Above this temperature, the erosion damage decreases as the oxide becomes thick enough to be protective. For all the conventional materials and sprayed coatings tested at 315 °C, erosion by repeated impacts enhanced their oxidation. The extent of oxidation can be approximated by the difference in volume loss observed at 315 and 25 °C.

5. Conclusions

In a laboratory gas-blast erosion rig simulating the operating conditions of fans, the volume loss of arc-sprayed coatings produced by repeated impacts of iron ore particles at impact angles of 25 and 90° was evaluated at 25 and 315 °C and compared to conventional materials. Three arc-sprayed coatings exhibited lower volume losses than AISI 1045 steel at 25 °C (CW1, CW2, and CW3), and only two coatings exhibited slightly lower volume losses than 1045 steel at 325 °C (CW1 and CW3) for a low impingement angle. At the impact angle of 90°, no coating exhibited lower volume losses than 1045 steel, 316 stainless steel, and ETP copper for both testing temperatures of

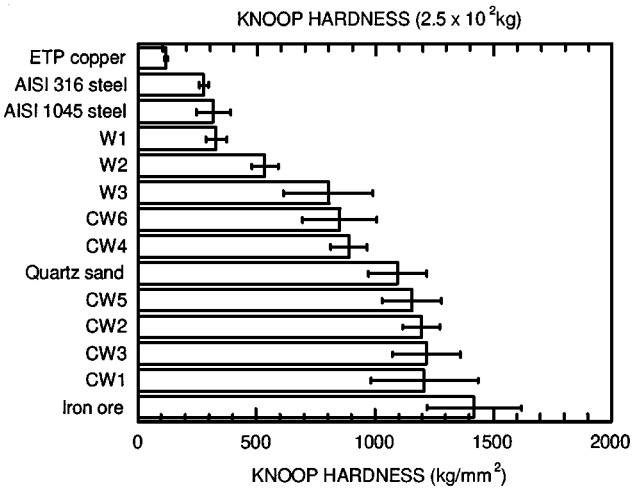

Fig. 21 Hardness of different materials and minerals

25 and 315 °C. Erosion enhanced oxidation to such an extent that nearly twice as much volume loss was observed at 315 °C than at 25 °C for both the sprayed coatings and conventional materials.

Though a few wires can be arc sprayed to form coatings that can mitigate the erosive action of coarse iron ore particles between 25 and 315 °C at low impact angles, no real benefit over structural steels is anticipated when erosion at both low and high impingement angles is considered. To combat erosion of components in devices operating at temperatures up to 600 °C (fans in processing industries, fossil-fired power plants, and fluidized bed combustors), new materials need to be developed.

Acknowledgments

The authors gratefully acknowledge the Quebec Cartier Mining Company and National Research Council Canada for financially supporting this work. The authors are also indebted to P. Gougeon and M. Lamontage for adapting the DPV-2000 apparatus to erodent velocity measurements and to M. Thibodeau for scanning electron micrography.

References

1. S. Dallaire, D. Dubé, and M. Fiset: *Wear*, 1999, vol. 231, pp. 102-07.
2. Anon: *Standard Practice for Conducting Erosion Tests by Solid Particle Impingement Using Gas Jets*, ASTM Designation G76, ASTM, Philadelphia, PA, 1992, pp. 301-05.
3. A.W. Ruff: *Wear*, 1986, vol. 108, pp. 323-35.
4. A. Levy and Y.-F. Man: *Wear*, 1986, vol. 111, pp. 135-59.
5. P.H. Shipway and I.M. Hutchings: *Wear*, 1994, vol. 174, pp. 169-75.
6. C.T. Morrison, R.O. Scattergood, and J.L. Routbort: *Wear*, 1986, vol. 111, pp. 1-13.
7. C. Moreau, P. Gougeon, M. Lamontagne, V. Lacasse, G. Vaudreuil, and P. Cielo: *Thermal Spray Industrial Applications*, Proc. 7th Thermal Spray Conf., Boston, MA, June 20–24, 1994, C.C. Berndt and S. Sampath, eds., ASM International, Materials Park, OH, 1994, pp. 431-37.
8. R.B. Bird, W.E. Stewart, and E.N. Lightfoot: *Transport Phenomena*, 7th ed., John Wiley & Sons, Inc., New York, NY, 1966.
9. P.H. Shipway and I.M. Hutchings: *Wear*, 1993, vol. 162-164, pp. 148-58.
10. S. Dallaire, M. Dufour, and B. Gauthier: *J. Thermal Spray Technol.*, 1993, vol. 2 (4), pp. 363-68.
11. A.R. Lansdown and A.L. Price: *Materials Resist Wear—A Guide to Their Selection and Use*, 1st ed., Pergamon Press, Oxford, United Kingdom, 1986.
12. L. Xu, C. Vose, and D. St.John: *Wear*, 1993, vol. 162-164, pp. 820-32.
13. *Source Book on Industrial Alloy and Engineering Data*, P.M. Untrweiser, ed., ASM International, Materials Park, OH, 1978.
14. Anon: *KM Mould Materials*, Brochure of KM-Kabelmetal, Osnabrück, Germany, 1994-1995.
15. A.V. Levy, J. Yan, and J. Patterson: *Wear*, 1986, vol. 108 (1), pp. 43–60.
16. C.B. Allen, T.F.J. Quinn, and J.L. Sullivan: *J. Tribol. (Trans. ASME)*, 1985, vol. 107 (2), pp. 172-79.
17. P.M. Rogers, T.E. Howes, I.M. Hutchings, and J.A. Little: *Wear*, 1995, vol. 164, pp. 148-58.
18. A.J. Ninham, I.M. Hutchings, and J.A. Litttle: *Corrosion*, 1990, vol. 46 (4), pp. 296-301.
19. B.Q. Wang, G.Q. Geng, and A.V. Levy: *Wear*, 1992, vol. 159, pp. 233-39.